Supporting Information

Untemplated Resveratrol-Mediated Polydopamine Nanocapsule Formation

Devang R. Amin[1,2], Cody J. Higginson[1], Angie Korpusik[1], Alyse R. Gonthier[1], Phillip B. Messersmith[1,3,*]

[1] Departments of Bioengineering and Materials Science and Engineering
University of California, Berkeley
210 Hearst Mining Building, Berkeley, CA 94720 United States

[2] Department of Biomedical Engineering
Northwestern University
2145 Sheridan Rd, Evanston, IL 60208 United States

[3] Materials Science Division
Lawrence Berkeley National Laboratory
Berkeley, CA 94720 United States

[*] Corresponding author: email: philm@berkeley.edu; ph: 510-643-9631

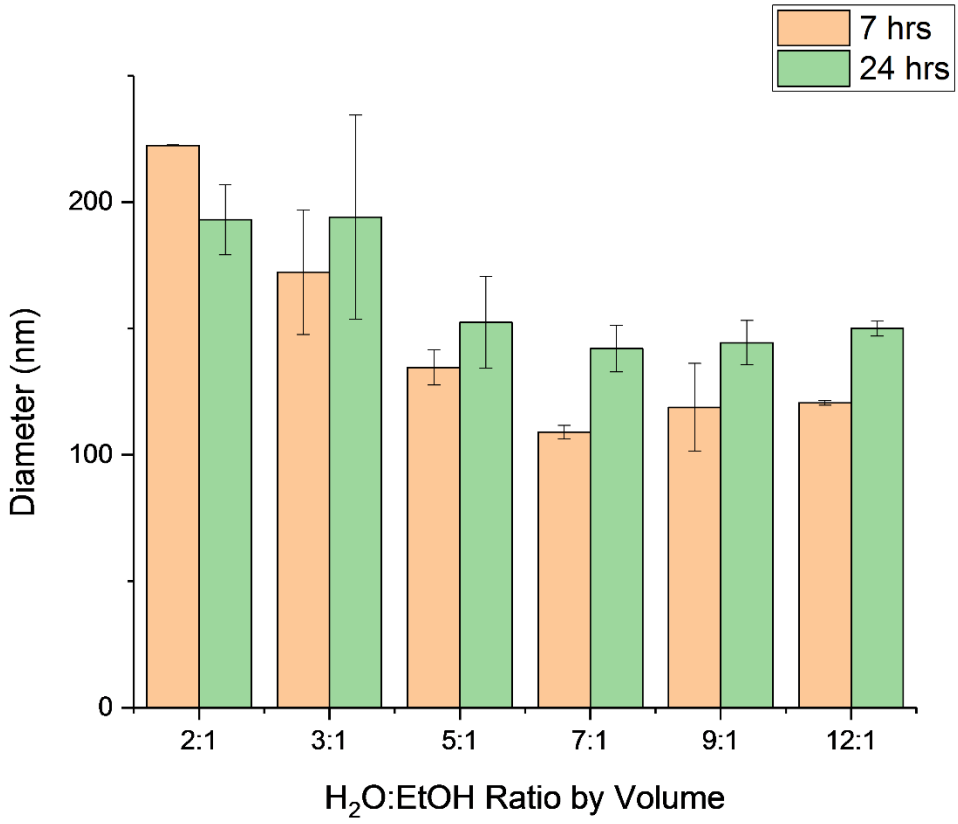

Figure S1: Hydrodynamic diameters of RV@PDA in solutions containing 0.125 mg/mL RV and 0.25 mg/mL DA after 7 h and 24 h of NP growth at various water:ethanol volume ratios. (Data collected from two independently prepared samples at each condition.)

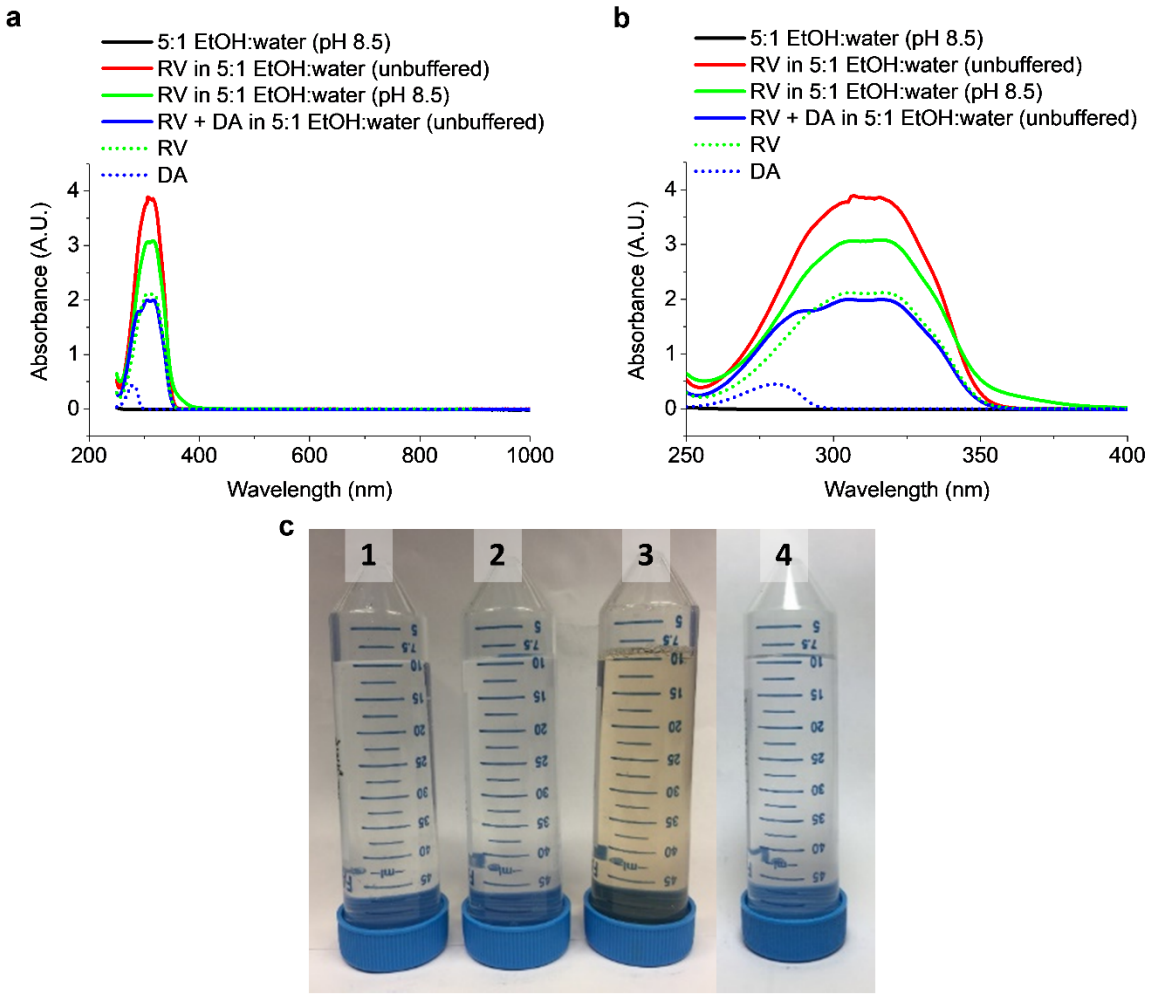

Figure S2: Visual and spectroscopic evaluation of RV and DA control solutions after 24h. (**a**) UV-Vis absorbance spectra of 0.25 mg/mL RV in 5:1 EtOH:water with or without pH 8.5 buffer and 0.125 mg/mL RV + 0.125 mg/mL DA in 5:1 EtOH:water after 24h. Spectra of freshly prepared 0.125 mg/mL RV and 0.25 mg/mL DA solutions in 5:1 EtOH:water are provided for reference. All solutions diluted 8 before obtaining spectra. (**b**) Spectra in (**a**) within the 250 nm – 400 nm wavelength range. (**c**) Visual appearance of 5:1 EtOH:water without buffer (**1**), 250 µg/mL RV in 5:1 EtOH:water without buffer (**2**), 250 µg/mL RV in 5:1 EtOH:water with pH 8.5 buffer (**3**), and 250 µg/mL DA + 125 µg/mL RV in 5:1 EtOH:water without buffer.

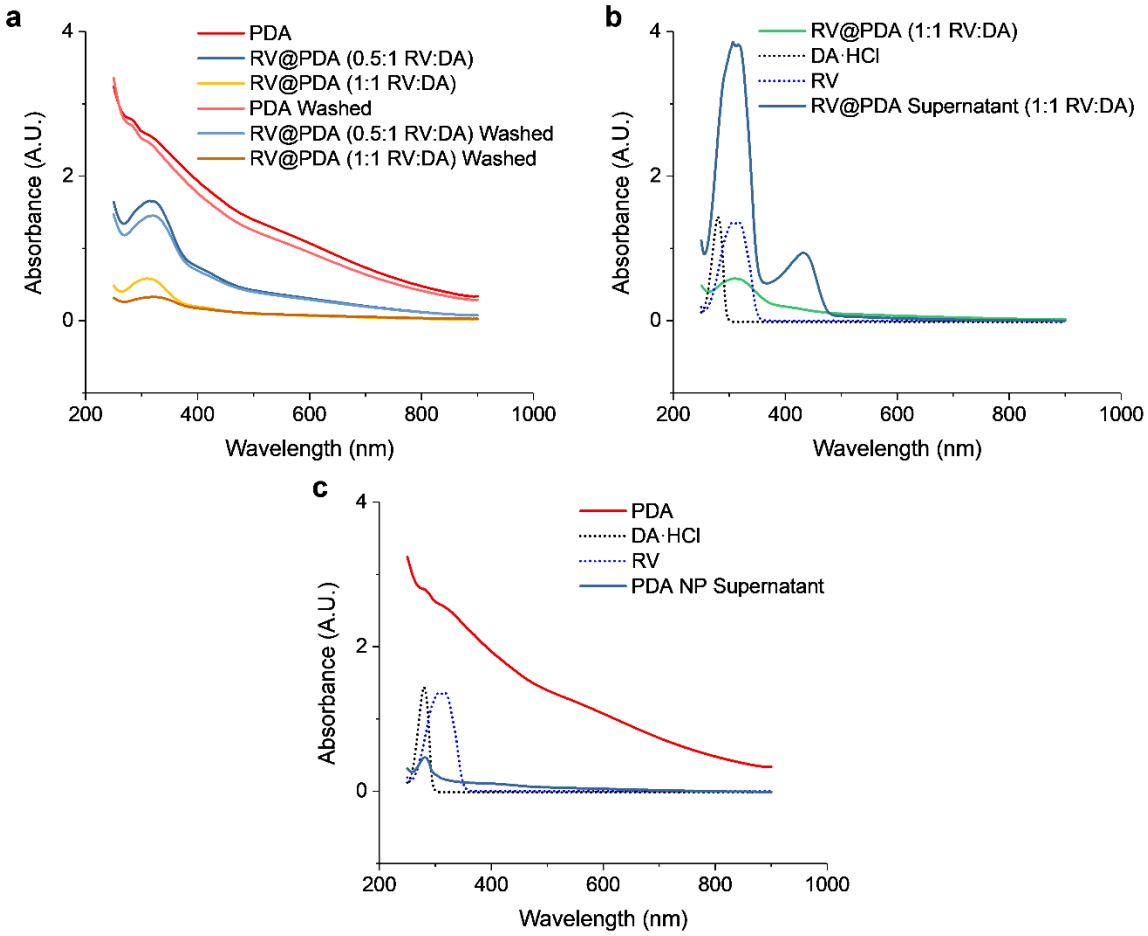

Figure S3: UV-Vis absorbance spectroscopy of PDA and RV@PDA. (**a**) Effect of washing nanomaterial product: spectra of pure PDA and RV@PDA before and after a third round of centrifugation. (**b-c**) Analysis of supernatants separated from pure PDA and RV@PDA product by centrifugation: (**b**) Spectra of pure RV@PDA prepared from 1:1 RV:DA in growth solution and the corresponding supernatant. (**c**) Spectra of pure PDA and the corresponding supernatant.

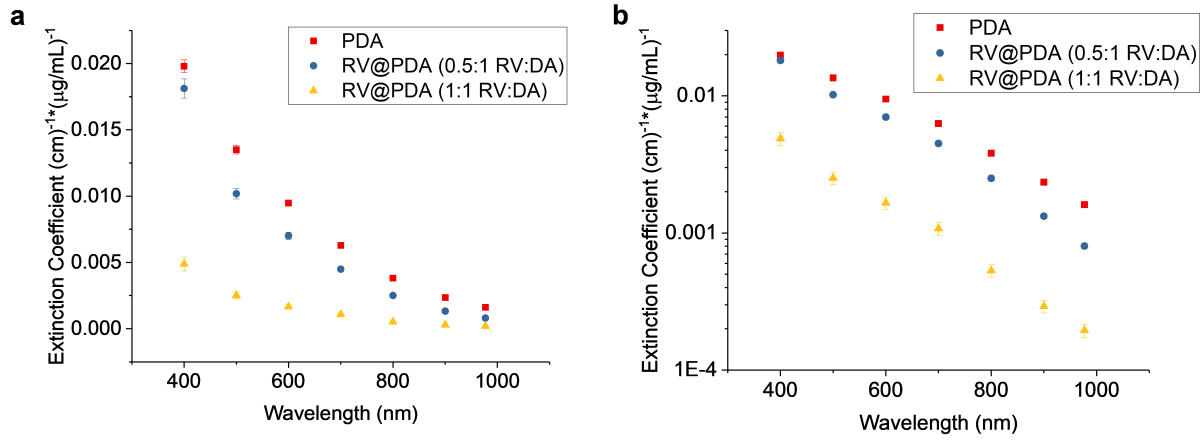

Figure S4: Extinction coefficients of PDA and RV@PDA from 400 nm – 977 nm. RV@PDA was prepared with either a 0.5:1 or 1:1 RV:DA mass ratio. (**a**) Extinction coefficients plotted vs. wavelength plotted with a linear y-axis. (**b**) Extinction coefficients vs. wavelength plotted with a logarithmic scale. Error bars represent the propagation of uncertainty in particle concentration.

Wavelength (nm)	PDA	RV@PDA (0.5:1 RV:DA)	RV@PDA (1:1 RV:DA)
400	$1.98 \times 10^{-2} \pm 4.74 \times 10^{-4}$	$1.81 \times 10^{-2} \pm 7.17 \times 10^{-4}$	$4.88 \times 10^{-3} \pm 5.18 \times 10^{-4}$
500	$1.35 \times 10^{-2} \pm 3.23 \times 10^{-4}$	$1.02 \times 10^{-2} \pm 4.03 \times 10^{-4}$	$2.51 \times 10^{-3} \pm 2.66 \times 10^{-4}$
600	$9.47 \times 10^{-3} \pm 2.27 \times 10^{-4}$	$7.00 \times 10^{-3} \pm 2.77 \times 10^{-4}$	$1.65 \times 10^{-3} \pm 1.75 \times 10^{-4}$
700	$6.29 \times 10^{-3} \pm 1.50 \times 10^{-4}$	$4.49 \times 10^{-3} \pm 1.78 \times 10^{-4}$	$1.07 \times 10^{-3} \pm 1.14 \times 10^{-4}$
800	$3.82 \times 10^{-3} \pm 9.14 \times 10^{-5}$	$2.50 \times 10^{-3} \pm 9.90 \times 10^{-5}$	$5.31 \times 10^{-4} \pm 5.63 \times 10^{-5}$
900	$2.34 \times 10^{-3} \pm 5.61 \times 10^{-5}$	$1.32 \times 10^{-3} \pm 5.24 \times 10^{-5}$	$2.92 \times 10^{-4} \pm 3.09 \times 10^{-5}$
977	$1.61 \times 10^{-3} \pm 3.85 \times 10^{-5}$	$8.03 \times 10^{-4} \pm 3.18 \times 10^{-5}$	$1.94 \times 10^{-4} \pm 2.06 \times 10^{-5}$

Table S1: Extinction coefficients (mean ± SD) plotted in Figure S3 for PDA and RV@PDA. Units are $cm^{-1} * (\mu g/mL)^{-1}$.

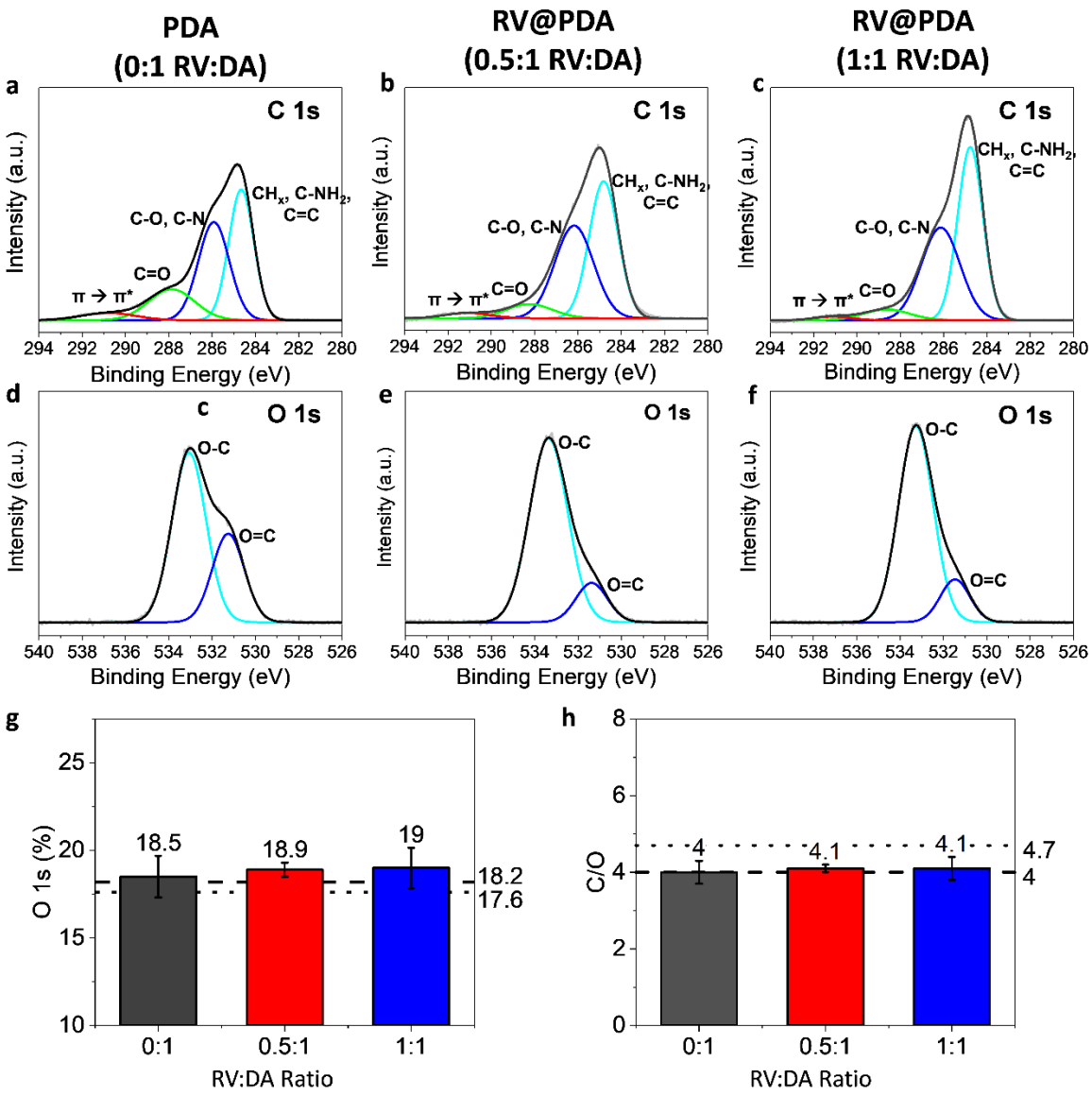

Figure S5: Analysis of high resolution XPS scans of PDA and RV@PDA nanomaterials. (**a-c**) C 1s peaks of PDA NPs (0:1 RV:DA) (**a**), RV@PDA with 0.5:1 RV:DA (**b**), and RV@PDA with 1:1 RV:DA (**c**). The deconvolution of this peak is shown, with energies corresponding to π- π* transition, C=O bonds, C-O and C-N bonds, and CH_x, C-NH_2, and C=C bonds labeled. (**d-f**) O 1s peaks of PDA (**d**), RV@PDA with 0.5:1 RV:DA (**e**), and RV@PDA with 1:1 RV:DA (**f**). Deconvolution into O-C and O=C bonding components is shown. (**g**) at% O calculated from analysis of high resolution O 1s scans relative to total C, N, and O content. (**h**) C/O atomic ratios calculated from high resolution C 1s and O 1s scans. Theoretical values of at% O and C/O ratio for DA (dashed lines) and RV (dotted lines) are shown for reference (**g-h**).

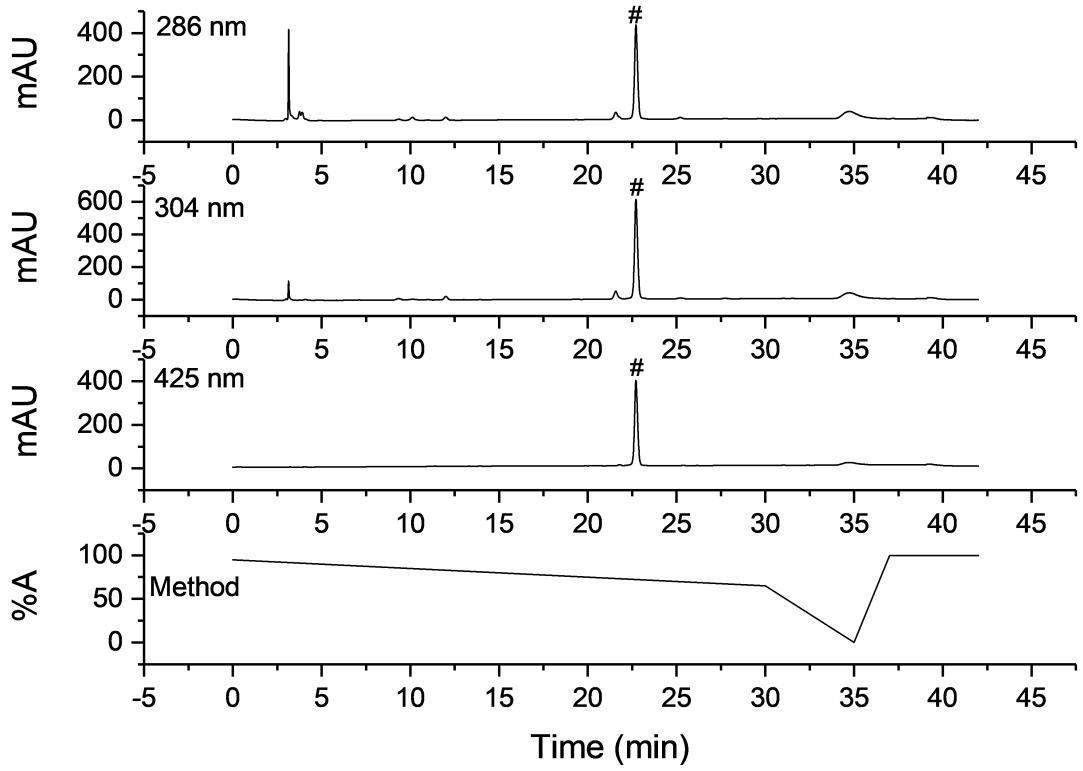

Figure S6: HPLC chromatographs of supernatant separated from RV@PDA nanomaterials (1:1 RV:DA) following 24h synthesis. Readouts from three UV-Vis detection wavelengths (286 nm, 304 nm, and 425 nm) are shown with the method for HPLC (%A: % ultrapure water + 0.1% TFA). The DA-RV adduct was identified by absorbance at 425 nm and elutes at 22.7 min (#). This compound was recovered for further analysis by ESI-MS, NMR, ATR-FTIR, and UV-Vis spectroscopy.

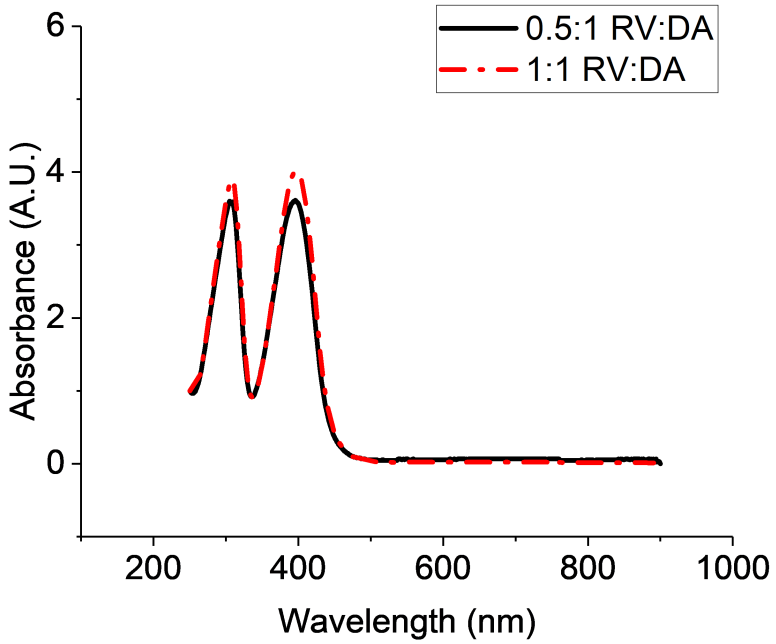

Figure S7: UV-Vis absorbance spectra of the dopamine-resveratrol adduct after purification by semiprep HPLC. The two curves shown correspond to product isolated from adduct formation in two reaction conditions (0.5:1 RV:DA and 1:1 RV:DA mass ratios). Both curves have absorbance maxima at λ_{abs} = 309 nm and λ_{abs} = 398 nm.

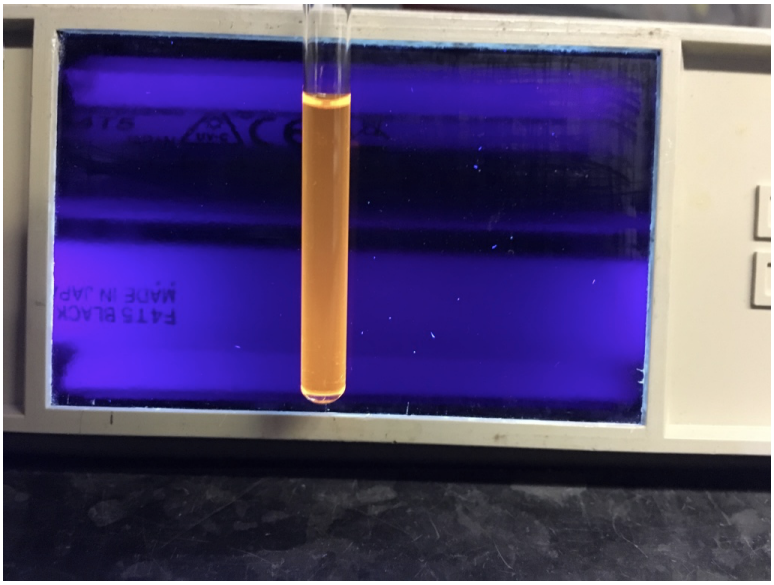

Figure S8: Fluorescence of pure dopamine-resveratrol adduct under long wave UV irradiation at 1 mg/mL in DMSO-d6.

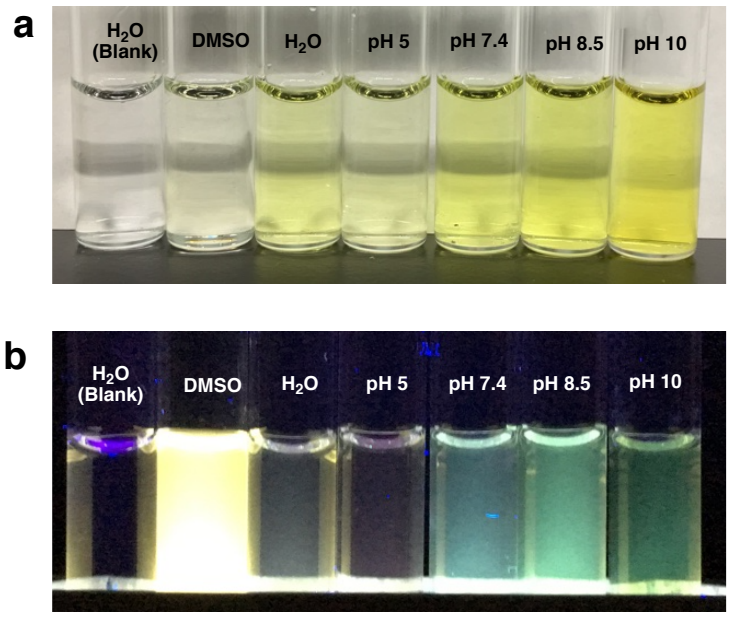

Figure S9: Optical properties of various resveratrol-dopamine adduct solutions at 0.02 mg/mL. Water blank is for visual reference. Samples were prepared by dilution of 1 mg/mL stock in DMSO-d_6 into the appropriate diluent. (**a**) Visible light image of solutions, (**b**) samples under longwave UV illumination. Buffer compositions were 0.1 M acetate (pH 5), 1x PBS (pH 7.4), 0.1 M bicine (pH 8.5), and 0.1 M sodium carbonate (pH 10).

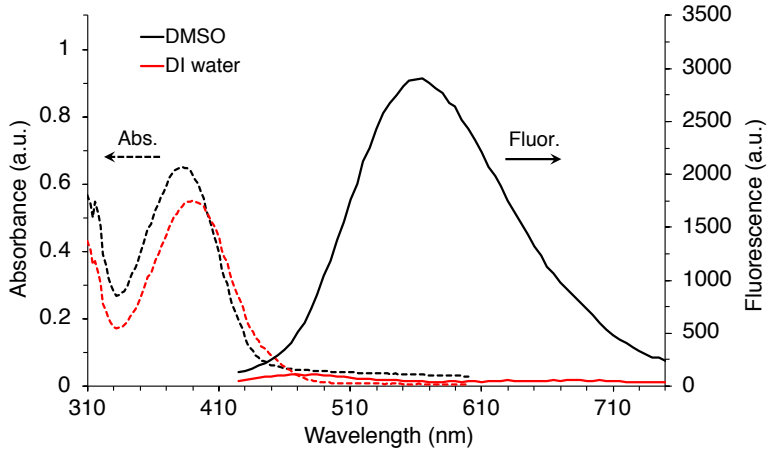

Figure S10: Absorbance and fluorescence spectra of 0.2 mg/mL dopamine-resveratrol adduct solutions in unbuffered DMSO and DI water (also pictured in Figure S9). Solutions were prepared from the trifluoroacetate salt of the adduct, isolated by semi-preparative HPLC in the presence of trifluoroacetic acid. Dotted lines represent absorbance (left axis), and solid lines represent emission (right axis, excitation at 390 nm).

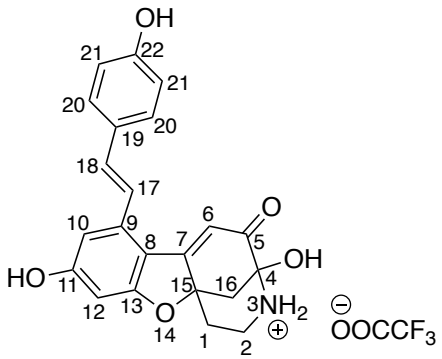

^{1}H NMR (900 MHz, DMSO-d_6) δ 10.86 (s, 1H, HO-C11), 9.81 (s, 1H, HO-C22), 9.41 (bs, 2H, NH_2•TFA), 7.85 (bs, 1H, HO-C4), 7.53 (d, J = 8.6 Hz, 2H, H20), 7.21 (d, J = 16.1 Hz, 1H, H17), 7.18 (d, J = 16.0 Hz, 1H, H18), 6.82 (d, J = 8.5 Hz, 2H, H21), 6.80 (d, J = 1.9 Hz, 1H, H10), 6.38 (d, J = 2.0 Hz, 1H, H12), 6.36 (s, 1H, H6), 3.28 (dd, J = 14.0, J = 5.6 Hz, 1H, H2a), 3.12 (app td, J = 13.7, J = 4.2 Hz, 1H, H2b), 2.70 (d, J = 12.0 Hz, 1H, H16a), 2.61 (dd, J = 11.9, 2.3 Hz, 1H, H16b), 2.16 (app td, J = 13.4, 5.7 Hz, 1H, H1a), 1.82 (app d, J = 13.2 Hz, 1H, H1b). ^{13}C NMR (226 MHz, DMSO) δ 188.61 (C5), 166.09 (C13), 165.20 (C11), 164.14 (C7), 158.37 (C22), 139.91 (C9), 134.07 (C18), 128.89 (C20), 127.20 (C19), 120.09 (H17), 115.74 (C21), 113.48 (C6), 110.29 (C8), 107.66 (C10), 96.66 (C12), 86.79 (C4), 82.77 (C15), 43.48 (C16), 36.44 (C2), 29.13 (C1).

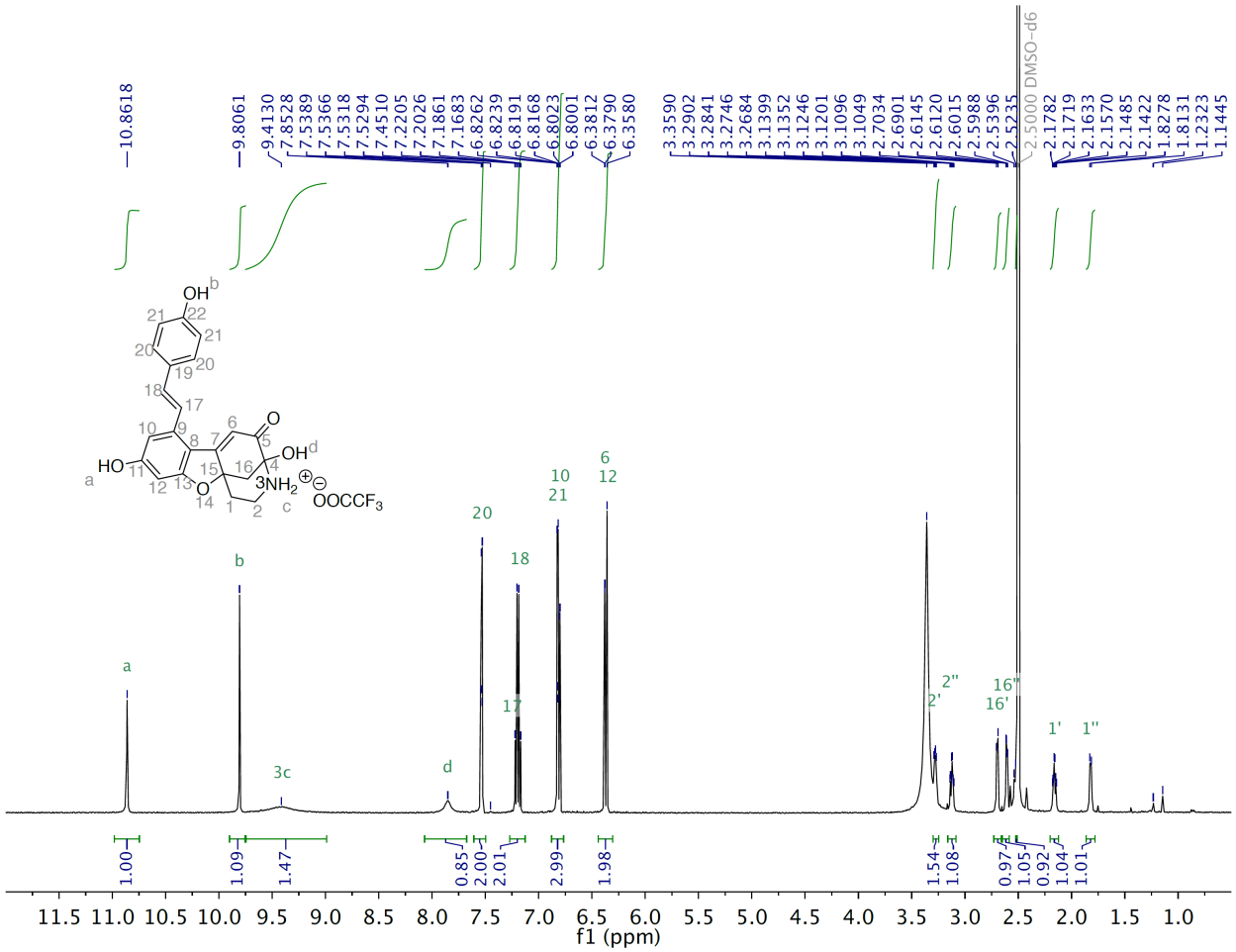

Figure S11: ^{1}H-NMR spectrum of isolated DA-RV adduct.

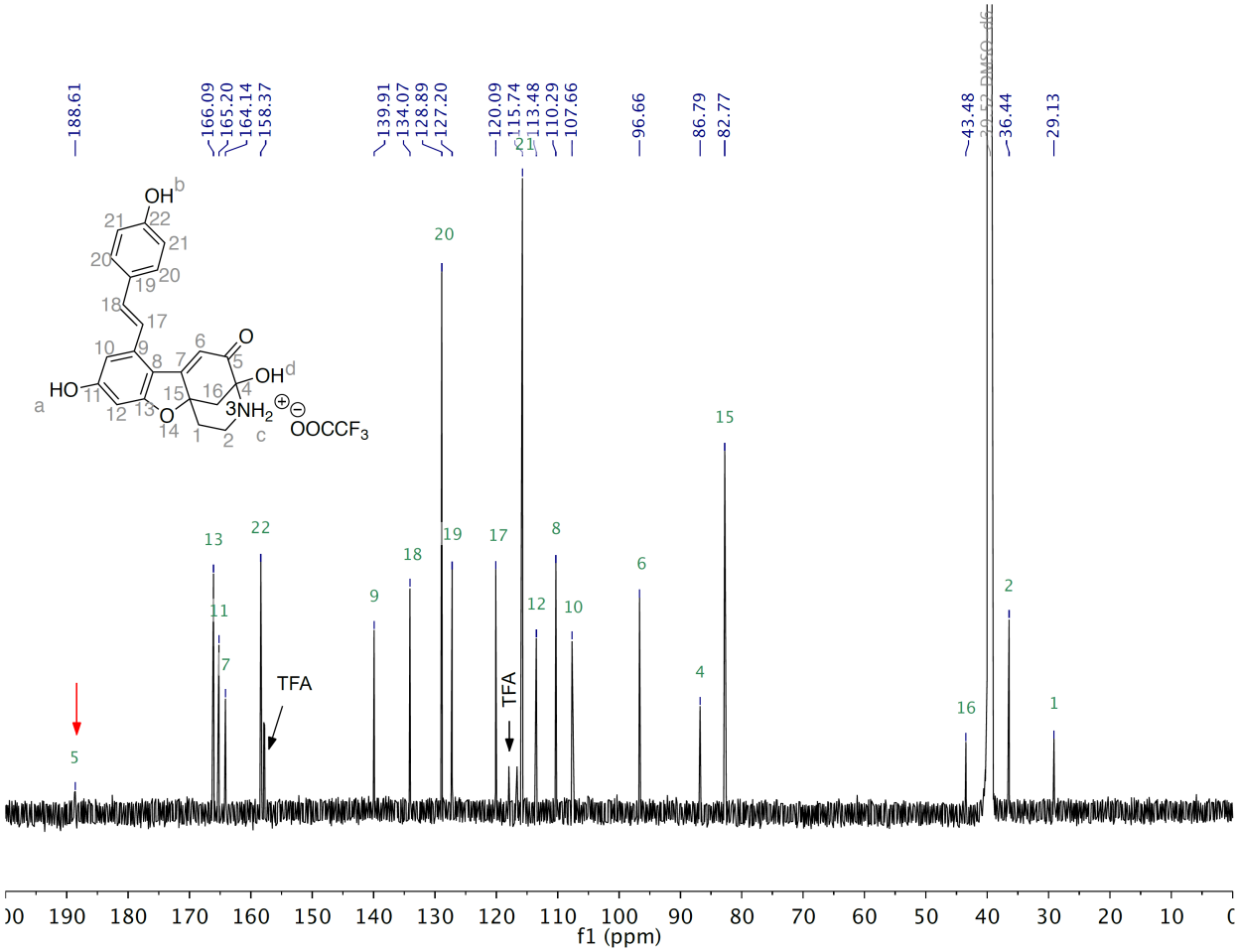

Figure S12: ^{13}C-NMR spectrum of isolated DA-RV adduct.

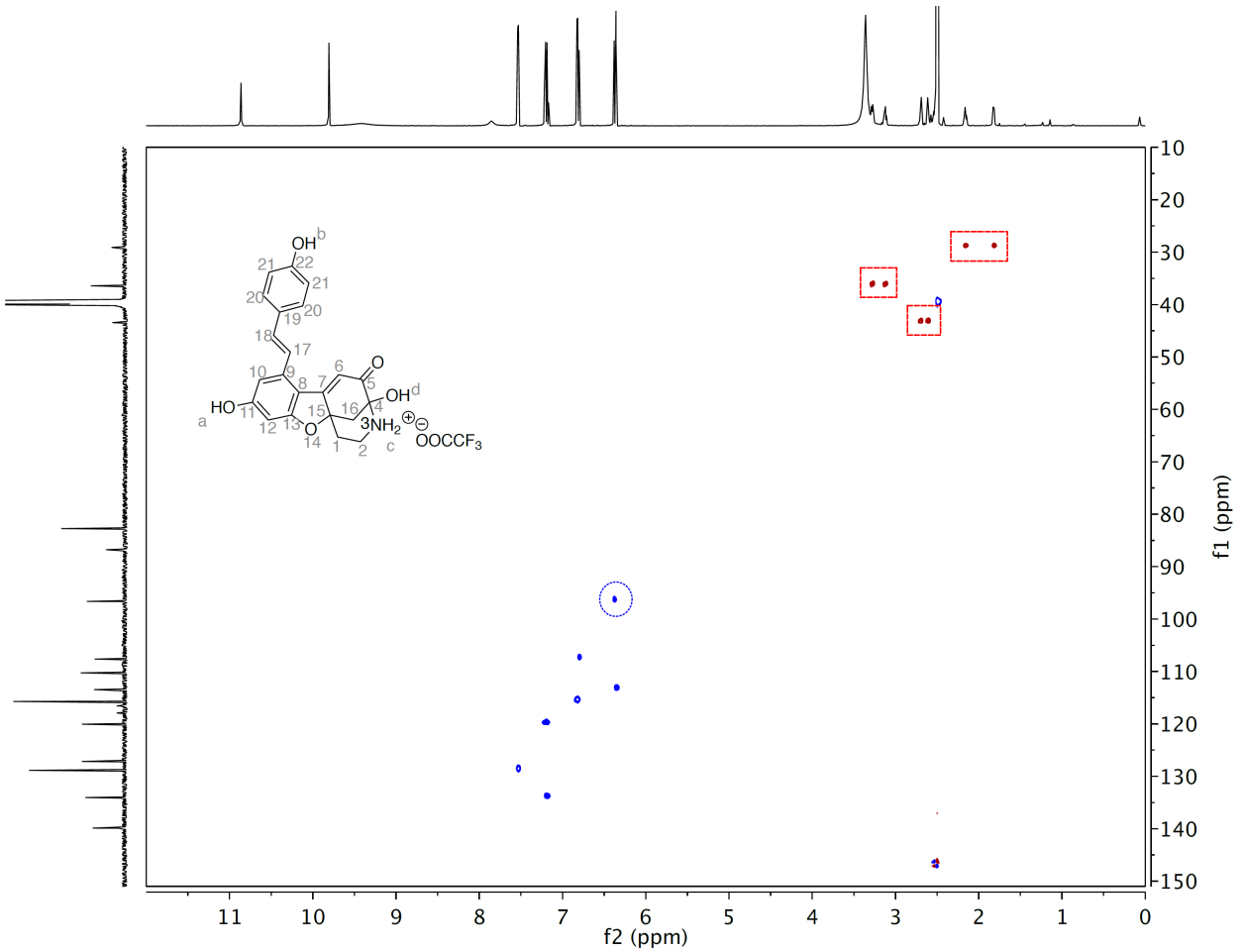

Figure S13: ^{1}H-^{13}C HSQC spectrum of isolated DA-RV adduct. Spectrum supports the presence of three methylene groups (red dashed boxes). Correlation of H6 and C6 is indicated by the blue dashed circle.

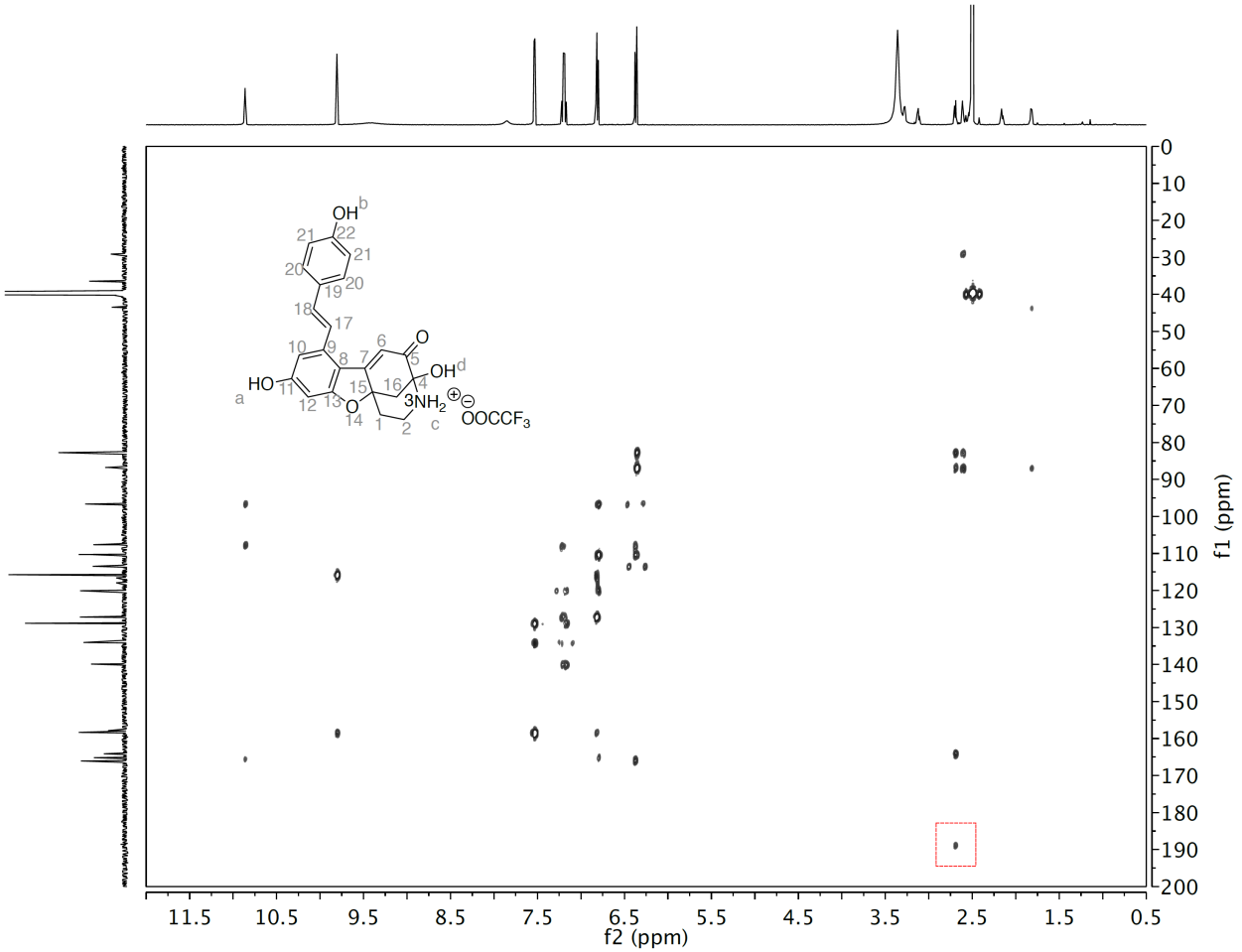

Figure S14: ^{1}H-^{13}C HMBC spectrum of isolated DA-RV adduct. Correlation between carbonyl C5 and proton H16" is indicated by the red dashed box.

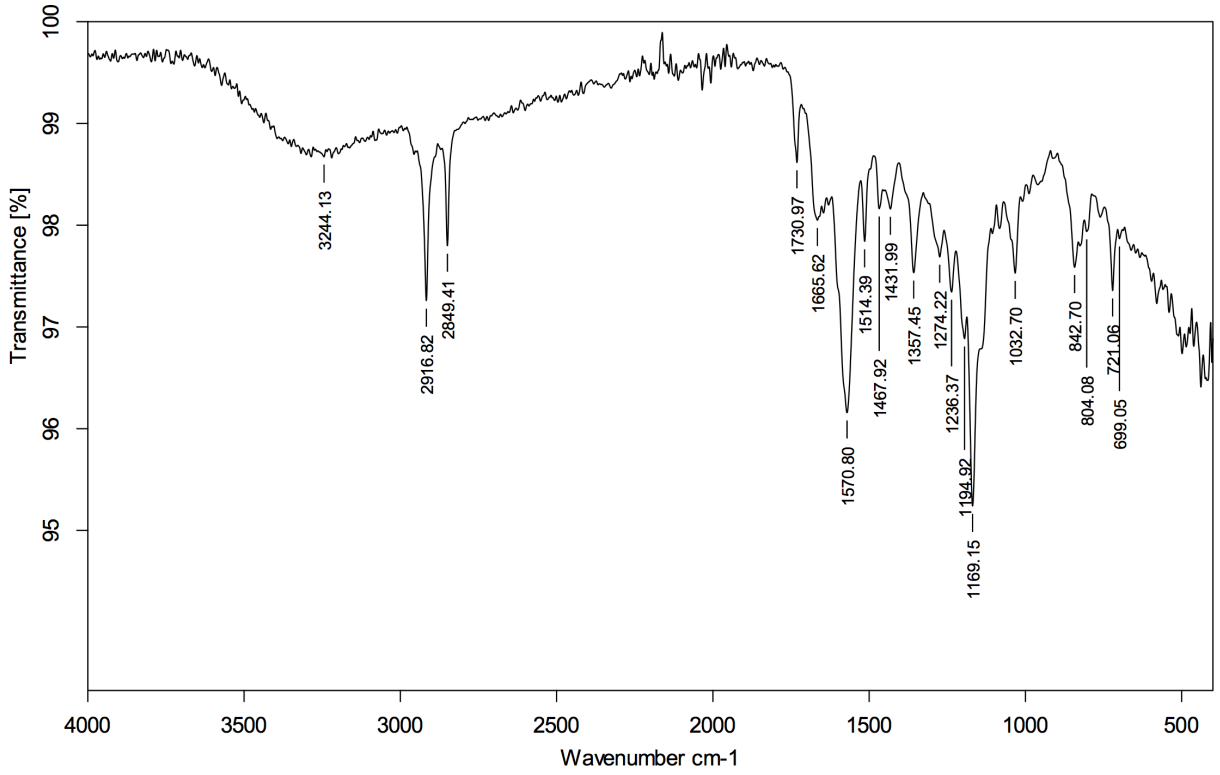

Figure S15: ATR-FTIR spectrum of solid HPLC-purified DA-RV adduct (256 scans).

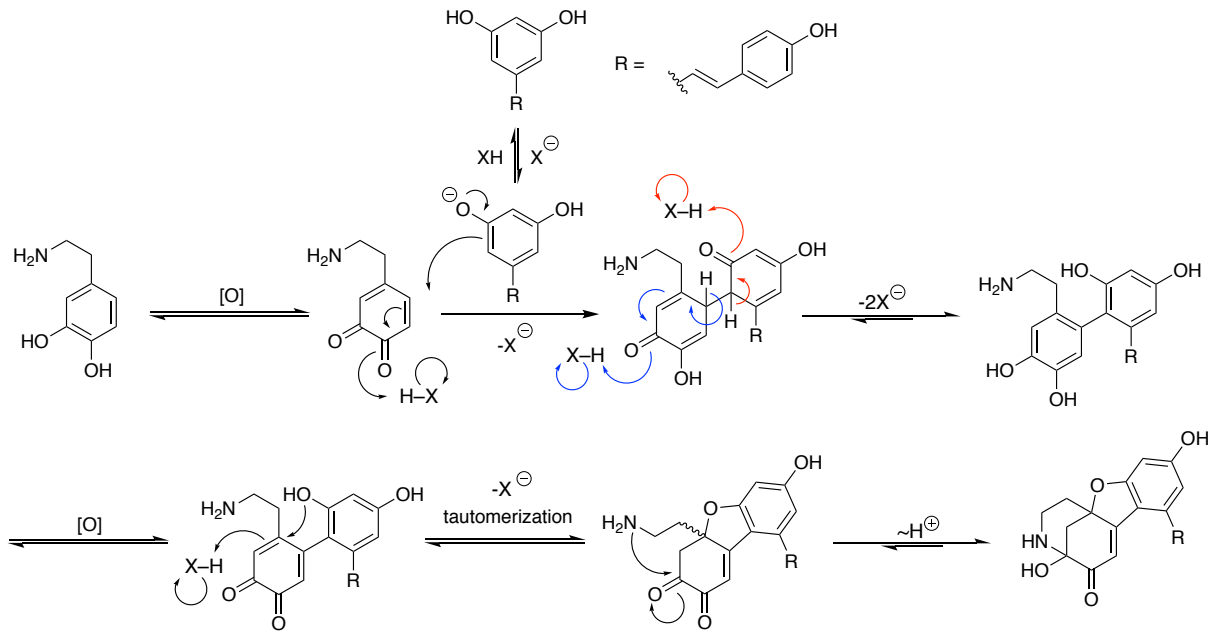

Figure S16: Plausible mechanism for formation of azamonardine DA-RV adduct.